International Journal of Orthopaedics

Online Submissions: http: //www.ghrnet.org/index.php/ijo
doi: 10.17554/j.issn.2311-5106.2022.09.454

Int. J. of Orth. 2022 June 28; **9(3)**: 1669-1675
ISSN 2311-5106 (Print), ISSN 2313-1462 (Online)

ORIGINAL ARTICLE

Computational Analysis of Strength and Fracture Location of Different Types of Femurs under Falling Condition using CT-Image based Finite Element Method

Zaw Linn Htun[1,3], Mitsugu Todo[1,2,] Manabu Tsukamoto[4], Takuaki Yamamoto[5], Masaaki Mawatari[6], Yasuharu Nakashima[7]

1 Interdisciplinary Graduate School of Engineering Sciences, Kyushu University, 6-1 Kasuga-koen, Kasuga, Fukuoka 816-8580, Japan;
2 Research Institute for Applied Mechanics, Kyushu University Kasuga-koen, Kasuga, Fukuoka 816-8580, Japan;
3 Department of Physics, University of Yangon, 11041 Kamayut, Yangon, Myanmar;
4 Department of Orthopaedic Surgery, University of Occupational and Environmental Health, 1-1 Iseigaoka, Yahatanishi-ku, Kitakyushu, Fukuoka 807-8555, Japan;
5 Department of Orthopedic Surgery, Fukuoka University, 7-45-1 Nanakuma, Jonan-ku, Fukuoka 814-0180 Japan;
6 Department of Orthopedic Surgery, Saga University, 5-1-1 Nabeshima, Saga 849-8501, Japan.
7 Department of Orthopaedic Surgery, Kyushu University, 3-1-1 Maidashi, Higashi-ku, Fukuoka 812-8580, Japan

Conflict-of-interest statement: The author(s) declare(s) that there is no conflict of interest regarding the publication of this paper.

Correspondence to: Mitsugu Todo, Interdisciplinary Graduate School of Engineering Sciences, Kyushu University, 6-1 Kasuga-koen, Kasuga, Fukuoka 816-8580, Japan.
Email: todo@riam.kyushu-u.ac.jp

Received: May 24, 2022
Revised: June 9, 2022
Accepted: June 10 2022
Published online: June 28, 2022

ABSTRACT

Sideways falling has been considered as a leading cause of hip fracture in elderly people with a high risk of morbidity and mortality. Therefore, early investigation of optimum femoral strength and fracture location of people at greatest risk can be clinically very useful for the preventive measures. It is also considered that some typical femoral diseases such as osteoarthritis (OA) and avascular necrosis (AVN) could affect the strength and fracture behaviour of the femurs. In this study, 130 computational femoral models were constructed using CT images of 73 patients. Then, CT image based finite element method combined with the damage mechanics analysis was applied to predict the fracture load as the femoral strength and the fracture location of the femoral models. The computational results exhibited that the fracture load tended to increase with increase of the volumetric bone mineral density estimated in the femoral head and neck region in all the three types of models. The bone fracture behaviour was expressed as expressed as the distribution of failure elements in the head and neck region. Under fall loading, the bone fracture mainly took place in the greater trochanter region for all types of femoral model. In addition, a combination of the greater trochanter and multifarious neck fracture was also observed in all the models. A combination of greater trochanter and intertrochanteric fracture was also observed in the AVN group.

Key words: Finite element analysis (FEA); Femoral strength; Fracture location; Osteoarthritis (OA); Avascular necrosis (AVN); Bone mineral density (BMD)

Htun ZL, Todo M, Tsukamoto M, Yamamoto T, Mawatari M, Nakashima Y. Computational Analysis of Strength and Fracture Location of Different Types of Femurs under Falling Condition using CT-Image based Finite Element Method. *International Journal of Orthopaedics* 2022; **9(3)**: 1669-1675 Available from: URL: http://www.ghrnet.org/index.php/ijo/article/view/3298

INTRODUCTION

Recent years, the risk of hip fractures in elderly people has dramatically increased due to the degradation of bone structure

caused by osteoporosis. A hip fracture can contribute a financial burden on patients, morbidity, and even mortality. Japan has the world's largest ageing population, and the number of hip fracture incidences in 2017 was estimated as about 193,400, consisting of 44,100 males and 149,300 females[1]. Cummings and other researchers also suggested that the number of patients with hip fractures might double or triple by the year 2040[2]. It is also reported by Asian Federation of Osteoporosis Societies (AFOS) that hip fracture incidences in Asian countries will increase up to 2.28-fold from 2018 to 2050[3].

With the hip fracture incidence increasing worldwide, for each of the osteoporotic patients, the estimation of fracture location and optimum strength of the femur have actively been performed. For example, the bone densitometry and the diagnostic imaging methods have generally been used to predict the risk of bone fracture. These methods usually provide regional bone density values for specific portions of the proximal femur and can visualize figures and shapes of the specific areas of the bone that may be related to the possibility of hip fracture[4,5]. However, these methods cannot provide a quantitative strength which is directly related to the fracture risk of the femur because the femoral strength depends on its 3D geometry, heterogeneity, distributed mechanical properties, and loading conditions.

In the meantime, a computer simulation method such as the CT-image based finite element method (CT-FEM) has been utilized to estimate the mechanical strength of femurs in order to assess the hip fracture risk of the elderly patient with osteoporosis[6-12]. Moreover, CT-FEM can analyse and predict not only the distributions of stress and strain within the bone model but also the fracture locations under the different boundary conditions[12-15].

Along with osteoporosis, some typical femoral diseases such as osteoarthritis (OA) and avascular necrosis (AVN) might significantly affect the femoral fracture behaviour and therefore the femoral strength; however, the effects of such diseases on the mechanical performance of femurs have not been investigated yet. In the present study, 3D computational finite element (FE) models of 130 femurs with healthy, OA and AVN conditions were constructed using CT images of lower limbs of 73 patients. Then, for each of the FE models, the mechanical testing was performed under a compressive loading condition in order to estimate its femoral strength and the fracture behaviour. Such fracture behaviour was recreated as the accumulation of failure elements under both the tensile and compressive stress conditions.

ANALYTICAL METHODS

Finite Element Modelling

Femoral CT data of 73 patients (10 men aged 37-75 years old, the average age of 51.49 years old, and 63 women aged 19-87 years old, the average age of 65.06 years old) were provided from four different university hospitals. A total of 130 computational femoral models were constructed using these CT images. Based on the patient's clinical data confirmed by orthopaedic surgeons, the 130 femurs were classified into three groups; 42 normal femurs (N1 group), 58 OA femurs (N2 group) and 30 AVN femurs (N3 group). The three different types of the femur are illustrated in Figure 1 and denoted by Normal, OA and AVN models, respectively, hereafter.

Three-dimensional numerical and finite element models of the femurs were constructed using Mechanical Finder v.11 (Research Center of Computational Mechanics Inc., Tokyo, Japan). Firstly, two-dimensional bone contours were extracted from the CT images, and then they were smoothly connected each other to construct three-dimensional femoral models. Then, the inside of each femoral model was filled with tetrahedral elements to create a finite element (FE) model[16]. The size of the tetrahedral elements was set to 2 to 4 mm. The whole surface of the FE model was also created using shell elements to imitate the stiff outer surface of the cortical bone with the greatest bone mineral density[17]. The average total number of the tetrahedral and the shell elements were roughly 178,000, and 28,000, respectively.

Mechanical Modelling and Material Properties

The tensile deformation behaviour of all the femoral bone models was assumed to be linear elastic characterized by two material parameters such as Young's modulus and Poisson's ratio, while their compressive deformation behaviour was assumed to be characterized by an elastic-plastic response with four material parameters such as Young's modulus, Poisson's ratio, yield strength and the work hardening coefficient.

For each of the tetrahedral elements, its mean bone mineral density (BMD) was firstly calculated from the corresponding CT value (CTv) by using the following linear equation[18-20]:

$$BMD = 0.001(CTv + 1.4246)/1.0580 \quad (1)$$

Where the units of BMD and CTv are given by g/cm^3 and Hounsfield Unit, respectively. Then Young's modulus of the element was estimated from the corresponding BMD by using the empirical formulae proposed by Keyak, et al[21]. For all the tetrahedral elements, Poisson's ratio was set to 0.4[6]. On the contrary, for all the shell elements, Young's modulus and Poisson's ratio were fixed to 20.6 GPa and 0.167, respectively. The distribution patterns of Young's modulus in the three femoral models presented in Figure 1 are shown in Figure 2. Distribution of the higher moduli corresponded to the location of cortical bone, while the lower moduli expressed cancellous bone and marrow.

Under the compressive deformation of all the elements, it was assumed that the onset of yielding took place when the Drucker-Prager equivalent stress reached the compressive yield strength (this is called 'Drucker-Prager yield criterion'). The yield strength of

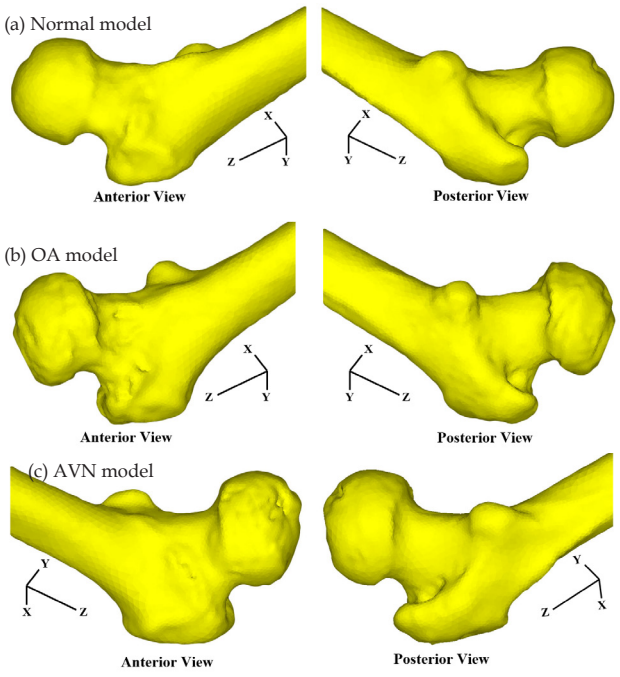

Figure 1 Three different types of femoral models.

each element was also obtained from the element's BMD by using the empirical formulae proposed by Keyak, et al[21], while the yield strength of all the shell elements was set to 20.6 MPa. The work hardening coefficient was set to 0.07 for all the elements.

In this FE analysis, bone fracture was reproduced as an aggregation of failure elements. Different failure criterions were used in the tensile and compressive stress conditions. Under the tensile stress condition, the maximum principal stress criterion was utilized to express the onset of localized tensile fracture of bone. It was assumed that the tensile failure of an element took place when the maximum principal stress reached its critical value, which was equal to 0.8 × (compressive yield strength)[12]. On the contrary, under the compressive stress condition, the minimum principal strain criterion was used to express the localized compressive bone fracture. It was assumed that the compressive failure of an element took place when the minimum principal strain reached its critical value which was equal to -10,000 μ strain, following the yielding of the element[22]. The failure of the element under both the tensile and compressive conditions was expressed by reducing the modulus down to the minimum value in the whole femoral model. The strength of the femoral model was then defined as a critical value of the applied load when 15 shell elements were failed[23].

Boundary Conditions

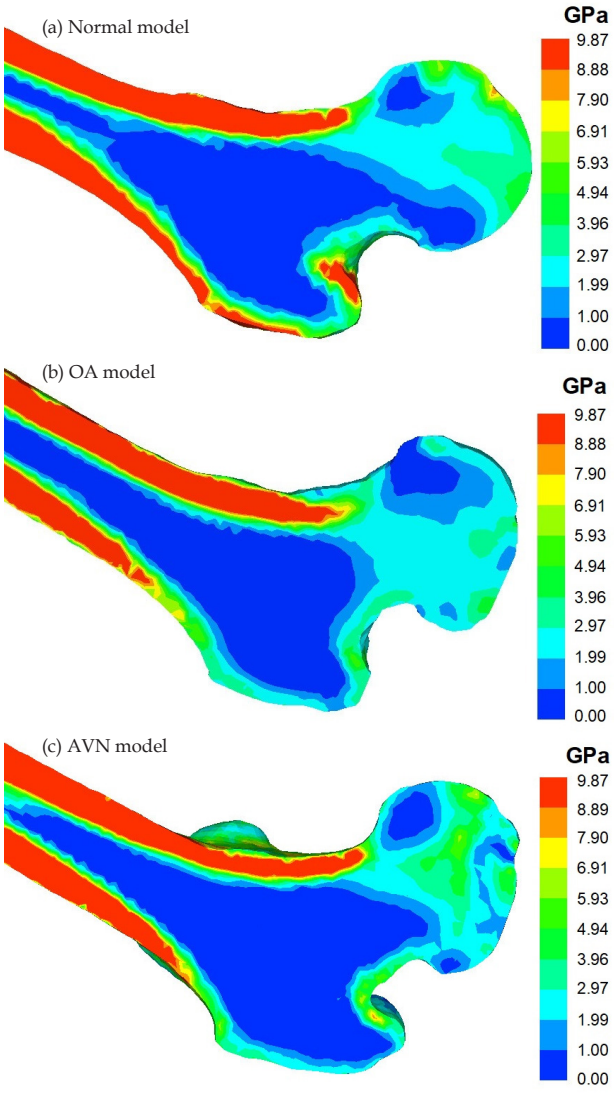

Figure 2 Distribution of Young's modulus in the cross-sectional area.

Firstly, the bone axes were set on the basis of the femoral method and then, the boundary conditions were determined accordingly. The boundary conditions, i.e., the fixed and loading conditions, are shown in Figure 3, respectively. As the fixed condition, the femoral surface from the bottom condylar surface to the circumferential line on the diaphysis located approximately 15 mm below the lesser trochanter was totally fixed as shown in Figure 3(a). The distributed load was applied to the femoral head vertically to the floor with the femoral shaft inclined by $\alpha = 60°$ and internally rotated by $\beta = 15°$ in reference to the floor as shown in Figure 3(b)[24,25]. The total value of the applied load was set to 10,000 N. The total load was divided into 10 main steps and each of the main steps was also divided into 4 sub-steps.

RESULTS AND DISCUSSION

Correlation Between Fracture Load and vBMD

The correlations between the fracture load and the average volumetric BMD (vBMD) of Normal, OA and AVN models are shown in Figure 4. For each of the models, a linear regression was fitted on the data and then Pearson's correlation coefficient was evaluated. Confidience interval (CI) statistics was also performed to precisely estimate the samples' mean and 95% predicted and 95% confidence bands of the fitted curve are also shown in Figure 4. The mean fracture loads of lower and upper 95% confidence interval and their descriptive statistical value for each femur type are listed in Table 1.

For Normal models shown in Figure 4(a), Pearson's correlation coefficient was found to be $r = 0.53$. Although the graphic data was widely scatterd, it could be said that the higher vBMD tended to reuslt in the higher fracture load. Confidience interval (CI) statistics was also performed to precisely estimate the samples' mean and 95% predicted and 95% confidence bands of the fitted curve are shown in Figure 4(a). The statistical results showed that the mean of 95% confidence interval was in a range from 896 ± 186 to 1,157 ± 151 N (mean ± standard deviation). This implyed that the mean fracture load of all 42 Normal models existed within this range with 95%

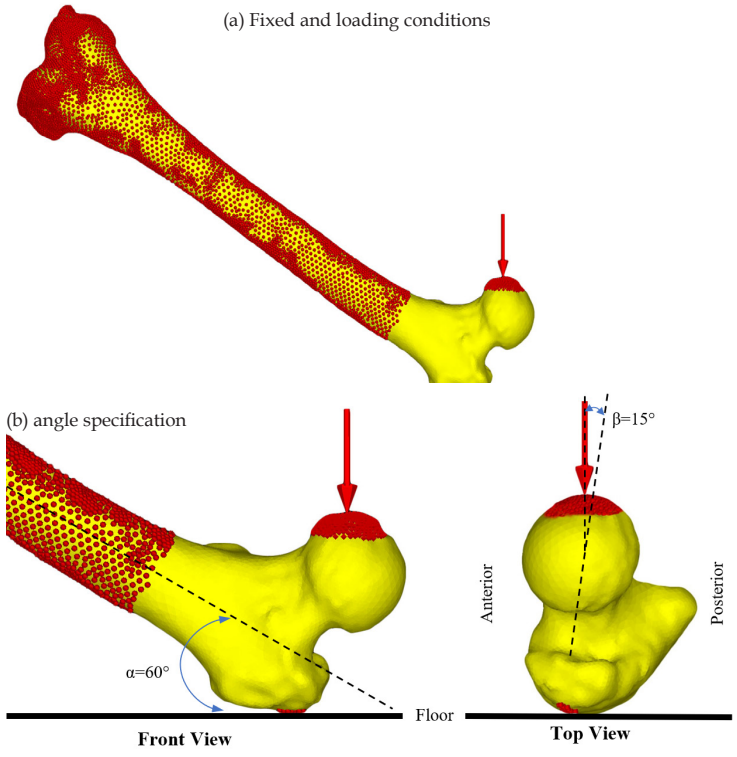

Figure 3 Boundary conditions imitating a falling condition.

confident.

For OA and AVN models shown in Figures 4(b) and (c), the Pearson's *r* values were found to be 0.42 and 0.43, respectively. 95% CI means were also observed in a range from 1,054 ± 154 to 1359 ± 170 N for OA models and from 962 ± 222 to 1,369 ± 166 N for AVN models. It is worth noting that the load ranges of OA and AVN models were apparently wider than that of the normal models. This fact could closely be related to the peculiar structural and mechanical properties of the OA and AVN femurs, depending on the extra bone growths induced by femoroacetabular impingement (FAI) in the OA femurs and various stages of collapsed femoral head surface in the AVN femurs[26]. The AVN femurs used in this study were classified into the 4 stages and therefore, the different stages could result in the broad range of fracture load.

Fracture Characteristics

For each femoral model, the fracture behaviour was expressed as the distribution of failure elements. For each of the three models, three different types of distribution partern of the failure elements are shown in Figure 5. Those microdamages consisted of three different failure modes, that is, tensile fracture (denoted by 'cracked element'), compressive yielding (denoted by 'plastic element'), and compressive fracture (denoted by 'crushed element'). The fracture regions were classified into 5 different types as shown in Table 2. It was noted that the bone fracture mainly took place in the greater trochanter region, secondly followed by a combination of greater trochanter and basicervical neck region for all the femoral models. In addition, a combination of the greater trochanter and either subcapital neck or transcervical neck fracture was also observed in all the models. Especially, this mixed fracture mode was mainly observed in OA models, showing 15 out of 58 models. On the other hand, a combination of the greater trochanter and intertrochanteric fracture was significantly occurred in AVN models. This type of unique fracture mode was only observed in AVN models (4 out of 30). More importantly, it was suggested from the simulation resutls that AVN femurs might fracture in all possible locations. It could be due to the variety of AVN stages. It is also to be noteworthy that the AVN femurs with potentially intertrochanteric fracture mixed with greater trochanter were of stage-3 and stage-4.

Table 1 Mean fracture loads of individual femoral group (unit: N).

Types of femur	Data	Mean	Standard Deviation	Minimum	Median	Maximum
Normal	Lower 95% Confidence Interval	896	186	513	945	1127
	Lower 95% Confidence Interval	1157	151	973	1108	1493
OA	Lower 95% Confidence Interval	1054	154	710	1109	1229
	Lower 95% Confidence Interval	1359	170	1163	1304	1724
AVN	Lower 95% Confidence Interval	962	222	504	1018	1237
	Lower 95% Confidence Interval	1369	166	1175	1314	1747

(a) Normal model

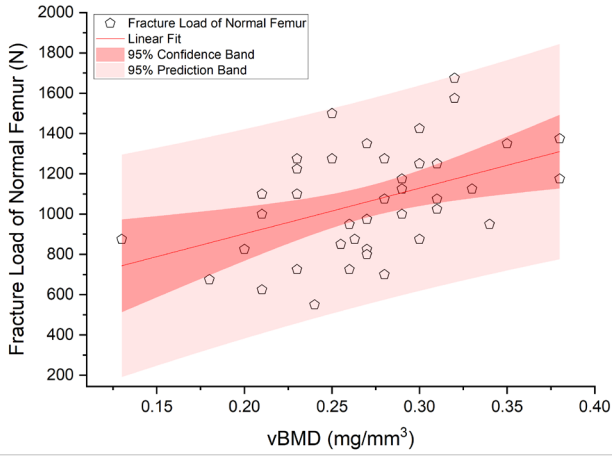

(b) OA model

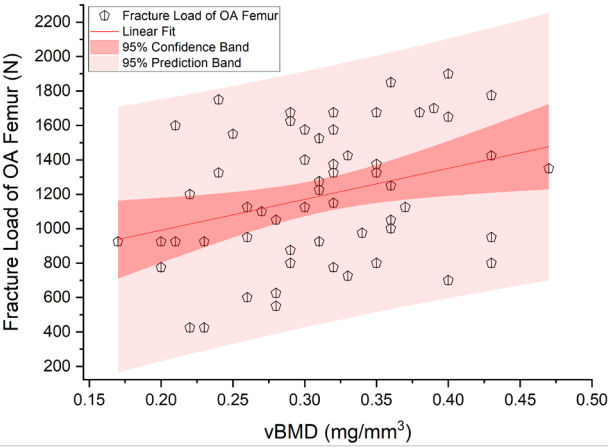

(c) AVN model

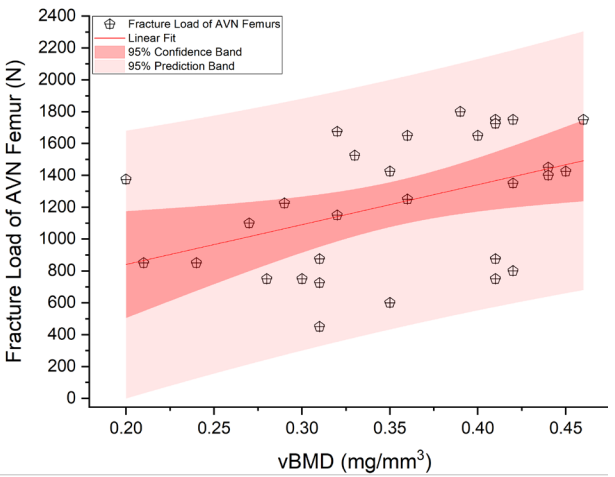

Figure 4 Correlation between fracture load and vBMD, including 95% interval of prediction band (pink color) and confidence band (light red color).

Table 2 Classification of fracture region.

Type of Femur (Sample Size)	Estimated Fracture Location				
	Greater Trochanter	Greater Trochanter + Neck (Subcapital)	Greater Trochanter + Neck (Transcervical)	Greater Trochanter + Neck (Basicervical)	Greater Trochanter + IntertrochantericRegion
Normal (N=42)	N=26 (61.9%)	N=3 (7.1%)	N=1 (2.4%)	N=12 (28.6%)	N=0
OA (N=58)	N=27 (46.5%)	N=12 (20.7%)	N=3 (5.2%)	N=16 (27.6%)	N=0
AVN (N=30)	N=14 (46.7%)	N=1 (3.3%)	N=1 (3.3%)	N=10 (33.3%)	N=4 (13.3%)

* Neck (Subcapital) = the femoral head and neck junction; * Neck (Transcervical) = the mid portion of femoral neck; * Neck (Basicervical) = the base of femoral neck

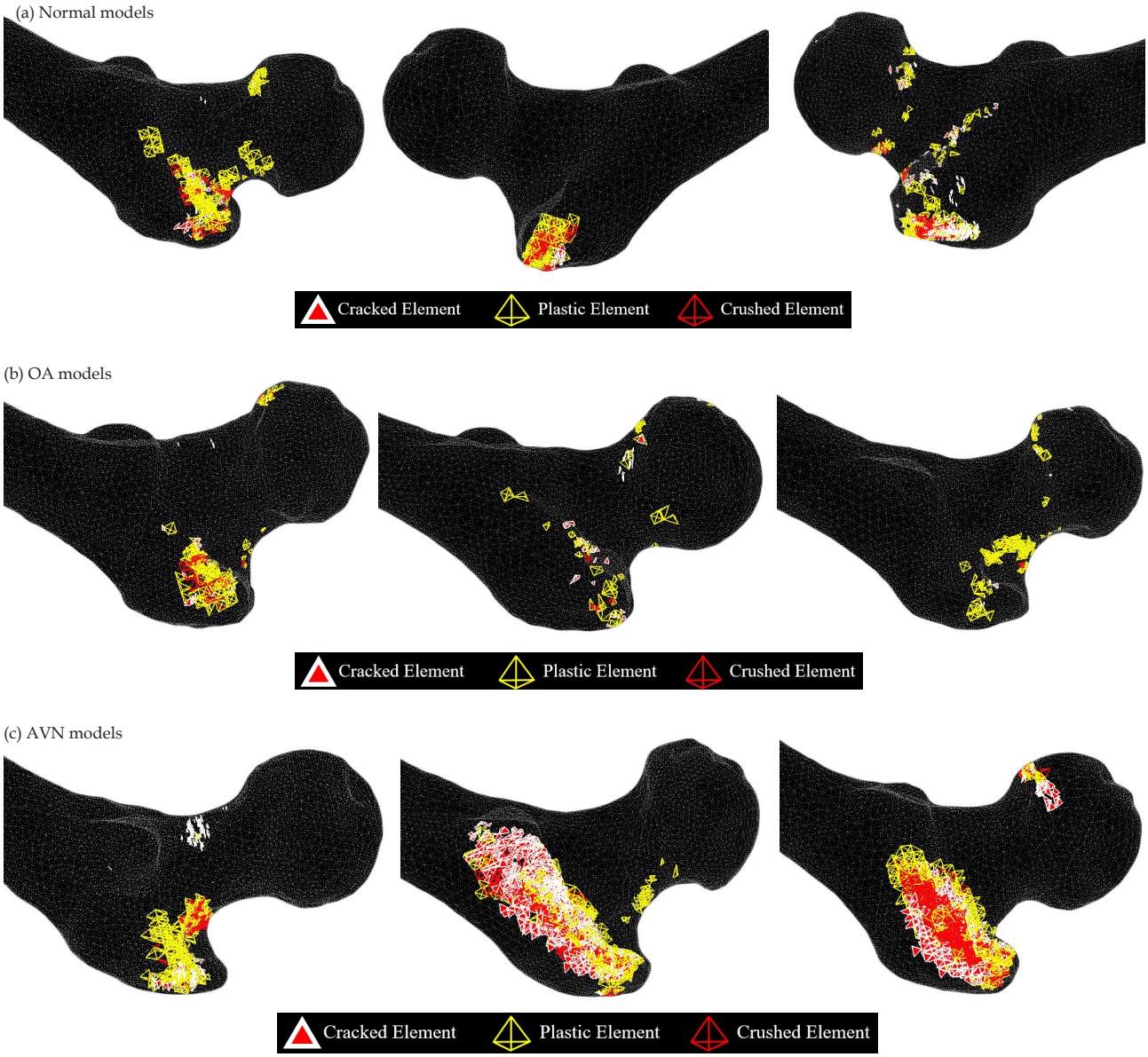

Figure 5 Three different types of bone fracture behaviour. Fracture patterns were expressed as the distribution of failure elements.

Comparison of Fracture Mechanism of Three models with same vBMD

Among all the 130 femoral models, it was found that some of them had the same vBMD with very different fracture load. In order to understand the difference in fracture mechanism, three models with the same vBMD of 0.32 mg/mm^3 were picked up and they are denoted by A-Normal, B-OA and C-AVN hereafter. The fractue load values of the three models were 1,650, 1,375, and 1,150 N, respectively. Their corresponding volumes of the head and neck region are compared in Figure 6, and it was clearly seen that A-Normal had the smallest volume with the highest femoral strength. On the contrary, B-OA and C-AVN had larger volumes with apparently lower fracture loads. It was therefore considered that the strength of femoral bone greatly depended on not only its geometry but also its microstructural parameters such as the distribution pattern of the mineral content.

For each of the three models, the accumulation of failure elements is shown as a function of load step in Figure 7. One step of load corresponded to 250 N. The strongest model, A-normal, reached up to 7 step, while the moderate model, B-OA, and the weakest

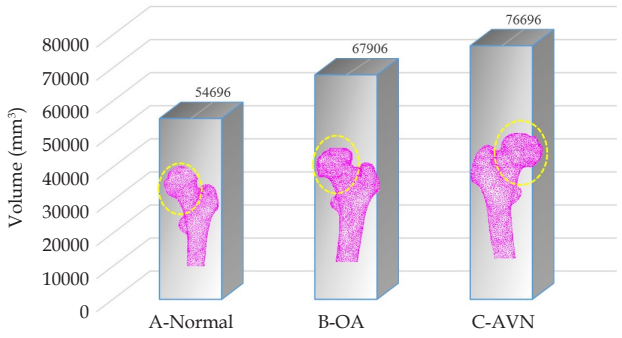

Figure 6 Comparison of the volume of the femoral head and neck region.

model, C-AVN, reached only 6 and 5 steps, respectively. Distribution patterns of strain energy density (SED) on the cross-sections of the three models at the fracture load are also shown in Figure 8. In A-normal and B-OA models, it was clearly seen that high SED smoothly distributed from the femoral head to the base of greater trochanter, suggesting an ideal propagation of mechanical stress and

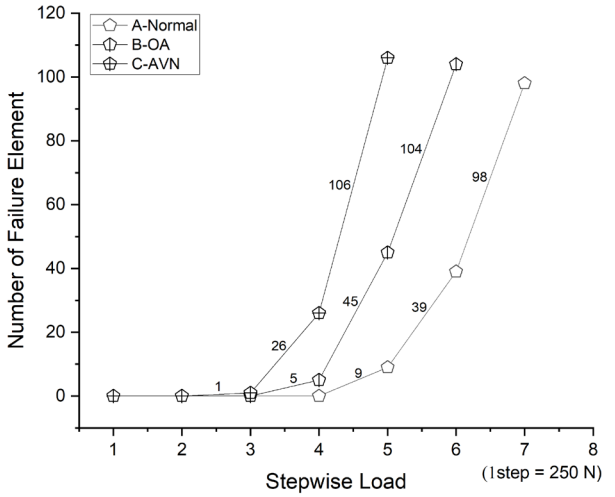

Figure 7 Accumulation of failure elements with increase of load steps in the three femoral models with the same vBMD.

resulting in the high fracture load. On the contrary, in C-AVN model, SED was largely concentrated on the greater trochanter region with low BMD, suggesting a higher risk of fracture.

CONCLUSIONS

In this study, three different groups of computational femoral model were constructed using CT data of normal, OA and AVN femurs. Then, the fracture load as the patient-specific femoral strength and the fracture location were analysed under the fall loading condition using the finite element method combined with the damage mechanics. The conclusions were obtained as follows:

(1) The fracture load tended to increase with increase of the average vBMD of the head and neck region with wide scatters. The Pearson's *r* values of Normal, OA and AVN models were evaluated as 0.53, 0.42 and 0.43, respectively, corresponding to the wider scatters observed in OA and AVN models than in Normal models.

(2) The bone fracture behaviour was expressed as the distribution of failure elements in the neck and trochanteric regions. It was noted that the bone fracture mainly took place in the greater trochanter region for all three models. In addition, a combination of the greater trochanter and neck fracture was also observed in all the models.

(3) A combination of greater trochanter and intertrochanteric fracture was also observed in AVN models, associated with disease levels of stage-3 and stage-4.

(4) Three models, A-normal, B-OA and C-AVN, with the same vBMD were compared. C-AVN exhibited the lowest fracture load with unnatural SED distribution which concentrated on the greater trochanter side, indicating a higher risk of fracture than the other regions.

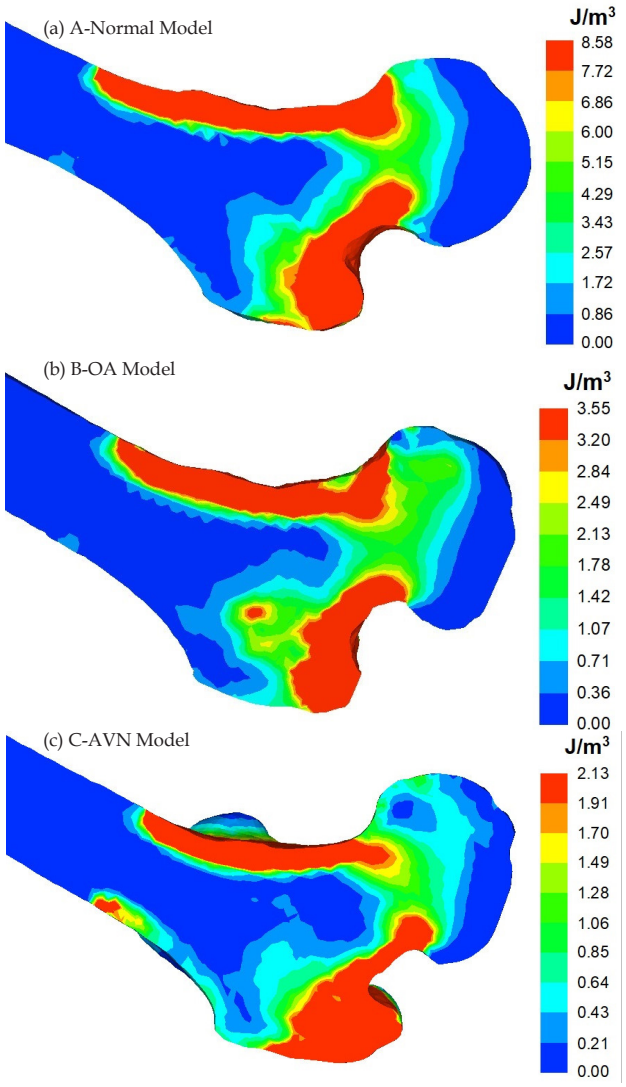

Figure 8 SED distribution patterns of three femoral models with the same vBMD.

REFERENCES

1. Takusari E, Sakata K, Hashimoto T, Fukushima Y, Nakamura T, Orimo H. Trends in Hip Fracture Incidence in Japan: Estimates Based on Nationwide Hip Fracture Surveys From 1992 to 2017. *JBMR Plus.* 2020; **5(2)**: e10428. [DOI: 10.1002/jbm4.10428]
2. Cummings SR, Rubin SM, Black D. The future of hip fractures in the United States. Numbers, costs, and potential effects of postmenopausal estrogen. *Clinical Orthopaedics and Related Research.* 1990; **(252)**: 163-6. [PMID: 2302881]
3. Cheung CL, Ang S Bin, Chadha M, Chow ESL, Chung YS, Hew FL, Jaisamrarn U, Ng H, Takeuchi Y, Wu CH, Xia W, Yu J, Fujiwara S. An updated hip fracture projection in Asia: The Asian Federation of Osteoporosis Societies study. *Osteoporosis and Sarcopenia.* 2018; **4(1)**: 16-21. [DOI: 10.1016/j.afos.2018.03.003]
4. Cummings SR, Browner W, Cummings SR, Black DM, Nevitt MC, Browner W, Genant HK, Cauley J, Ensrud K, Scott J, Vogt TM. Bone density at various sites for prediction of hip fractures. The Study of Osteoporotic Fractures Research Group. *The Lancet.* 1993; **341(8837)**: 72-5. [DOI: 10.1016/0140-6736(93)92555-8]
5. Lang TF, Keyak JH, Heitz MW, Augat P, Lu Y, Mathur A, Genant HK. Volumetric quantitative computed tomography of the proximal femur: Precision and relation to bone strength. *Bone.* 1997; **21(1)**: 101-8. [DOI: 10.1016/S8756-3282(97)00072-0]
6. Keyak JH, Rossi SA, Jones KA, Skinner HB. Prediction of femoral fracture load using automated finite element modeling. *Journal of Biomechanics.* 1997; **31(2)**: 125-33. [DOI: 10.1016/S0021-9290(97)00123-1]
7. Ota T, Yamamoto I, Morita R. Fracture simulation of the femoral bone using the finite-element method: How a fracture initiates and proceeds. *Journal of Bone and Mineral Metabolism.* 1999; **17(2)**: 108-12. [DOI: 10.1007/s007740050072]
8. Cody DD, Gross GJ, Hou FJ, Spencer HJ, Goldstein SA, Fyhrie DP. Femoral strength is better predicted by finite element models than QCT and DXA. *Journal of Biomechanics.* 1999; **32(10)**: 1013-20. [DOI: 10.1016/S0021-9290(99) 00099-8]

9. Keyak JH, Rossi SA, Jones KA, Les CM, Skinner HB. Prediction of fracture location in the proximal femur using finite element models. *Medical Engineering and Physics.* 2001; **23(9)**: 657-64. [DOI: 10.1016/S1350-4533(01)00094-7]
10. Bessho M, Ohnishi I, Matsuyama J, Matsumoto T, Imai K, Nakamura K. Prediction of strength and strain of the proximal femur by a CT-based finite element method. *Journal of Biomechanics*. 2007; **40(8)**: 1745-53. [DOI: 10.1016/ j.jbiomech.2006.08.003]
11. Gustafsson A, Tognini M, Bengtsson F, Gasser TC, Isaksson H, Grassi L. Subject-specific FE models of the human femur predict fracture path and bone strength under single-leg-stance loading. Journal of the Mechanical Behavior of Biomedical Materials. 2021; **113**: 104118. [DOI: 10.1016/j.jmbbm.2020.104118]
12. Abdullah AH, Todo M, Nakashima Y. Prediction of damage formation in hip arthroplasties by finite element analysis using computed tomography images. *Medical Engineering and Physics.* 2017; **44**: 8-15. [DOI: 10.1016/ j.medengphy.2017.03.006]
13. Cristofolini L, Schileo E, Juszczyk M, Taddei F, Martelli S, Viceconti M. Mechanical testing of bones: The positive synergy of finite-element models and in vitro experiments. *Philosophical Transactions of the Royal Society A: Mathematical, Physical and Engineering Sciences.* 2010; **368(1920)**: 2725-63. [DOI: 10.1098/ rsta.2010.0046]
14. Todo M. Biomechanical Analysis of Hip Joint Arthroplasties using CT-Image Based Finite Element Method. *Journal of Surgery and Research.* 2018; **1(2)**: 34-41. [DOI: 10.26502/jsr.1002005]
15. Nor Izmin NA, Hazwani F, Todo M, Abdullah AH. Fracture Analysis of Resurfaced Femur with Varus Implant Placement. *Proceedings of International Exchange and Innovation Conference on Engineering & Sciences (IEICES).* 2021; **7**: 7-12. [DOI: 10.5109/4738551]
16. Ulrich D, van Rietbergen B, Weinans H, Rüegsegger P. Finite element analysis of trabecular bone structure: A comparison of image-based meshing techniques. *Journal of Biomechanics*. 1998; **31(12)**: 1187-92. [DOI: 10.1016/ S0021-9290(98)00118-3]
17. Dalstra M, Huiskes R, van Erning L. Development and validation of a three-dimensional finite element model of the pelvic bone. *Journal of Biomechanical Engineering.* 1995; **117(3)**: 272-8. [DOI: 10.1115/1.2794181]
18. Hirata Y, Inaba Y, Kobayashi N, Ike H, Yukizawa Y, Fujimaki H, Tezuka T, Tateishi U, Inoue T, Saito T. Correlation between mechanical stress by finite element analysis and 18F-fluoride PET uptake in hip osteoarthritis patients. *Journal of Orthopaedic Research.* 2015; **33(1)**: 78-83. [DOI: 10.1002/jor. 22717]
19. Miyamura S, Oka K, Abe S, Shigi A, Tanaka H, Sugamoto K, Yoshikawa H, Murase T. Altered bone density and stress distribution patterns in long-standing cubitus varus deformity and their effect during early osteoarthritis of the elbow. *Osteoarthritis and Cartilage.* 2018; **26(1)**: 72-83. [DOI: 10.1016/j.joca. 2017.10.004]
20. Kitamura K, Fujii M, Utsunomiya T, Iwamoto M, Ikemura S, Hamai S, Motomura G, Todo M, Nakashima Y. Effect of sagittal pelvic tilt on joint stress distribution in hip dysplasia: A finite element analysis. *Clinical Biomechanics.* 2020; **74**: 34-41. [DOI: 10.1016/j.clinbiomech.2020.02.011]
21. Keyak JH, Skinner HB, Fleming JA. Effect of force direction on femoral fracture load for two types of loading conditions. *Journal of Orthopaedic Research.* 2001; **19(4)**: 539-44. [DOI: 10.1016/ S0736-0266(00)00046-2]
22. Sato T, Yonezawa I, Todo M, Takano H, Kaneko K. Biomechanical Effects of Implant Materials on Posterior Lumbar Interbody Fusion: Comparison of Polyetheretherketone and Titanium Spacers Using Finite Element Analysis and Considering Bone Density. *Journal of Biomedical Science and Engineering.* 2018; **11(04)**: 45-59. [DOI: 10.4236/jbise.2018.114005]
23. Oba M, Kobayashi N, Inaba Y, Choe H, Ike H, Kubota S, Saito T. Mechanical Strength of the Proximal Femur After Arthroscopic Osteochondroplasty for Femoroacetabular Impingement: Finite Element Analysis and 3-Dimensional Image Analysis. *Arthroscopy - Journal of Arthroscopic and Related Surgery.* 2018; **34(8)**: 2377-86. [DOI: 10.1016/j.arthro.2018.03.036]
24. Bessho M, Ohnishi I, Matsumoto T, Ohashi S, Matsuyama J, Tobita K, Kaneko M, Nakamura K. Prediction of proximal femur strength using a CT-based nonlinear finite element method: Differences in predicted fracture load and site with changing load and boundary conditions. *Bone*. 2009; **45(2)**: 226-31. [DOI: 10.1016/j.bone.2009.04.241]
25. Abdullah AH, Todo M, Nakashima Y, Iwamoto Y. Risk of Femoral Bone Fractures in Hip Arthroplasties during Sideway Falls. *International Journal of Applied Physics and Mathematics*. 2014; **4(4)**: 286-9. [DOI: 10.7763/ijapm.2014. v4.300]
26. Murphey MD, Roberts CC, Bencardino JT, Appel M, Arnold E, Chang EY, Dempsey ME, Fox MG, Fries IB, Greenspan BS, Hochman MG, Jacobson JA, Mintz DN, Newman JS, Rosenberg ZS, Rubin DA, Small KM, Weissman BN. ACR Appropriateness Criteria Osteonecrosis of the Hip. *Journal of the American College of Radiology.* 2016; **13(2)**: 147-55. [DOI: 10.1016/j.jacr. 2015.10.033]